Series Editor
Robert Baptist

Wide Band Gap Semiconductor Nanowires 2

Heterostructures and Optoelectronic Devices

Edited by

Vincent Consonni
Guy Feuillet

ISTE

WILEY

4 ZnO and GaN Nanowire-based Type II Heterostructures

4.1. Semiconductor heterostructures

We can hardly find one functional semiconductor device that does not involve at least one hetero-junction that either serves as an active component of the device (e.g. a charge separating interface in a solar cell) or provides a supporting role (e.g. passivating the surface of the active material). The behavior or function of the hetero-junction depends critically on a physical quantity called band offset that describes the relative energy-level alignment or band alignment between the two materials. The significance of band offset is well highlighted by H. Kroemer's Lemma of Proven Ignorance [KRO 02]: "If you cannot draw an Energy Band Diagram, this shows you don't know what you are talking about", because the band offset is the key information for drawing the band diagram. With this said, the accurate information about the band offset between two materials of interest is not always known precisely. There are various theoretical and experimental results available in the literature, which most of the time agree qualitatively but not quantitatively [VAN 03, LI 09]. Uncertainty in the order of tens to one hundred meV is typical for most materials. However, it has been well established that there are three basic types of band alignments as depicted in Figure 4.1: type I, type II(a) and type II(b), in terms of the relative energy levels of the conduction band minimum (CBM) and valence band maximum (VBM) of the two materials. If we define $\Delta E_c = E_{CBM,1} - E_{CBM,2}$ and $\Delta E_v = E_{VBM,1} - E_{VBM,2}$, ΔE_c and ΔE_v will have opposite signs for type I, same signs for types II(a) and II(b). The difference between type II(a) and

Chapter written by Yong ZHANG.

type II(b) lies in that in type II(b) the CBM of one of them is so low that it is even below the VBM of the other material.

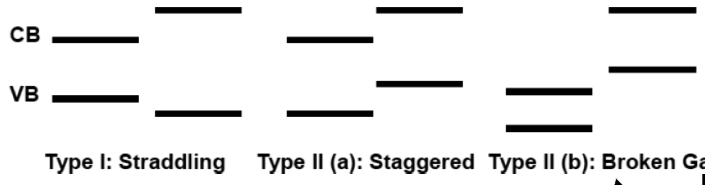

Figure 4.1. *Three basic types of hetero-junction band alignments*

The best known example for type I is perhaps GaAs/AlGaAs in which AlGaAs is expected to stop both the electron and hole respectively near the GaAs CBM and VBM to enter AlGaAs because of the barriers for both the electron and hole. However, by doping GaAs and AlGaAs simultaneously the same type, either n or p type, one of the electron or hole barriers can be substantially reduced, but not both. If they are doped in opposite types, we will have a heterostructure p–n junction in which both barriers are increased from the respective values when the materials are un-doped. For type II(a), the electron and hole will normally be separated into two materials, with the electron in the left and the hole in the right for the arrangement depicted in Figure 4.1, much like in a simple p–n junction, but without the need for doping. For type II(b), as in type II(a), the electron and hole tend to be separated. However, because the original fully occupied valence band of the material to the right now has its VBM above the CBM of the empty conduction band (CB) of the material to the left, charge transfer from the higher VBM side to the CBM of the other material may occur, even if both materials are un-doped and without external excitation. If following the convention defining the bandgap as the energy difference between the lowest empty s-like band edge and the highest occupied p-like band edge, we would say that the type II(b) heterostructure has a negative bandgap as a system. Type I band alignment has been widely used in light-emitting devices such as LED and semiconductor lasers in the form of a double heterostructure such as AlGaAs/GaAs/AlGaAs with the intent to contain the injected carriers, electrons and holes to the active layer of GaAs to promote radiative recombination. Type II(b) band alignment has been found useful in the form of a super-lattice, such as a periodic structure of InAs/GaSb with a few nm thick for each layer, as the active layer of an IR detector in mid-wave or long-wave spectral ranges. The quantum confinement of GaSb to the electron in InAs and of InAs to the hole in GaSb will increase the bandgap of the type II(b) system from a negative value (when the layers

are thick) to in principle any desirable small but positive bandgap. However, type II(a) band alignment has not been recognized to have any significant application in semiconductor technologies.

4.2. Type II heterostructures

We can easily notice that from Figure 4.1 the type II(a) band alignment qualitatively resembles a p–n junction, i.e. electrons will tend to follow or stay in left side of the junction, and holes on the right side. In short, it has the ability to separate the electron and hole. In principle, this is a much more abrupt or sharp junction than a p–n junction. The width of a p–n junction is determined by the doping level of the layers, and limited by the achievable doping level, which makes it practically difficult to reduce the junction width to the scale, typically of more than few tens of nm in a semiconductor, at which quantum effects become significant. Perhaps due to the huge success of all the p–n junction-based semiconductor technologies, the potential of such an abrupt junction has not been explored substantially. Given the important role of the p–n junction in semiconductor devices and the great interest in nanoscale semiconductor devices, the type II(a) junction should be given more attention in the exploration of future generation nanotechnologies.

The charge separation function of the type II(a) interface has been utilized in two well-known solar cell technologies both involving organic materials where doping is generally found very challenging: (1) the organic solar cell (often known as bulk hetero-junction solar cell, BHJSC) [NEL 01] and (2) dye-sensitized solar cell (DSSC)[GRA 05]. There are in fact two all-inorganic variations of DSSC: (1) extremely thin absorber (ETA) solar cell [FRN 03] and (2) quantum dot-sensitized solar cell (QDSSC) [YU 06] (for more details, we refer to Chapter 10). We note that in all these cases, usually the lower bandgap component, for instance the dye molecule, plays the primary role of light absorber, whereas the other component with a larger bandgap mostly serves the role of a conducting electrode. The photo-response threshold E_{PRT} in energy or λ_{PRT} in wavelength, is practically determined by the bandgap of the lower bandgap component. To some extent, these solar cells are similar to an inorganic p-i-n solar cell with a low-conductivity absorber layer. Strictly speaking, the DSSC, of which the name was probably given based on the phenomenological observation of the sensitization effect, should really be called a "dye solar cell" in the same sense we would call a GaAs solar cell with a doped AlGaAs electrode layer a "GaAs solar cell" rather than a "GaAs-sensitized solar cell". This clarification is not meant to suggest the need to change the names for these well-known technologies but to offer the necessary context for introducing an

all-inorganic type II(a) solar cell technology that is distinctly different from ETA cell and QDSSC. In contrast to BHJSC, DSSC, ETA cell and QDSSC where the E_{PRT} of the device is determined for all practical purposes by the bandgap of the lower bandgap material, the E_{PRT} for an IR detector based on the InAs/GaSb type II(b) super-lattice is determined jointly by the electronic structures of the two components and can be much smaller than any of the individual bandgaps. Although the wave functions of the electron and hole are respectively more localized in InAs and GaSb, there is sufficient overlapping that can offer decent strength absorption (e.g. ~1000 cm^{-1}) near the fundamental bandgap of the super-lattice [MOU 09]. The absorption might still be more than one order in magnitude weaker than that of a direct bandgap semiconductor but already more than two orders in magnitude stronger than that of an indirect bandgap semiconductor. The absorption in such type II(b) super-lattice could be thought of as originating from the interfacial transition that is substantially enhanced by the quantum mechanical coupling between the two materials. Semiconductor heterostructures in general have the advantage of being relatively easy to engineer the interfacial coupling. For a molecular system such as BHJSC, there is actually a similar interfacial effect, known as a charger-transfer exciton state (a state localized at the interface), that can also lead to photo-response below the bandgaps of the individual components unfortunately it is extremely weak and thus would not make any meaningful contribution to the device [CLA 10].

The focus of this chapter is to describe a new approach that employs two large bandgap materials with type II(a) band alignment to achieve near-IR or visible photo-response threshold that is desired in solar energy applications, such as solar cell and photo-chemical cell, and other optoelectronic applications [ZHA 07]. The material combinations of particular interest may include GaN/GaP for III-Vs, ZnO/ZnSe, ZnO/ZnTe and ZnO/ZnS for II-VI's, because individually none of these components would be considered viable to efficiently capture the solar spectrum. Other possible combinations may include GaN/GaAs, ZnO/CdSe, ZnO/CdTe, CdSe/CdTe and CdS/ZnTe, involving smaller bandgap materials. Most of these combinations are highly lattice mismatched between the two components, except for CdSe/ZnTe being near lattice matched. A type II(a) super-lattice of CdSe/ZnTe has been explored recently and shown to yield an effective bandgap below those of the individual components [BOY 12].

3. Optimal device architecture

It is quite apparent that a periodically stacked heterostructure or super-lattice of any of the three types most likely will have rather poor electronic conductivity along the stacking direction, unless the layers are made extremely thin, for instance, down

to a few mono-layers. Unfortunately in most practical applications, many mono-layers are required, including the example using type II(b) InAs/GaSb super-lattices for IR detection. Therefore, a compromise has to be made between optical absorption and electronic conductivity. An ideal situation would be having the super-lattice stacking direction perpendicular to that of the growth which is also normally the preferred direction of the electronic transport. In this way, the electron and hole can be separated laterally with short-traveling distances and extracted vertically without being blocked by the other layer. Furthermore, because the electron and hole are quickly separated spatially, the recombination loss could be reduced significantly. This idea can in principle be achieved by generating lateral composition modulation, which has been observed in various strained III-V alloys [MIL 97]. However, such spontaneously generated modulation tends to have a relatively low degree of structural perfection.

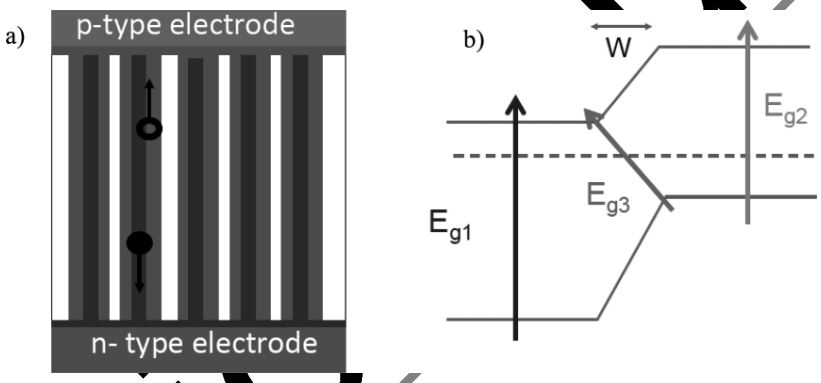

Figure 4.2. *Operation principle of core–shell NW array solar cell.a) Schematic of the device structure (one of the electrodes should be transparent); and b) band diagram showing three possible electronic transitions. The dashed line indicates the Fermi level at equilibrium. For a color version of this figure, see www.iste.co.uk/consonni/nanowires2.zip*

For a conventional planar semiconductor device, one apparent fundamental shortcoming in the device architecture is that it allows for and often requires carrier lateral motion, which increases carrier collection loss or poses a stringent requirement – long carrier diffusion length – to material quality. The simplest and generally adopted mitigation to the lateral transport loss (also known as sheet resistance loss) is the use of a fingered electrode on the side of the device for either in- or out-coupling of light in optoelectronic devices such as solar cells, LEDs and photo-detectors. A more sophisticated scheme has been developed for Si solar cells

to improve carrier collection: an array of inter-digitated back-contact function as quasi-lateral p–n junctions [SWA 86]. A quasi-one-dimensional (1D) system can take this idea one step further, which offers the possibility of exploring quantum effects and new functionalities in reduced dimensionality and novel device geometries, and material properties tailored to specific applications [ZHA 07]. It has been well established that for a semiconductor material with a given density of non-radiative centers, by restricting the carrier motion sequentially to more spatial dimensions, the non-radiative centers become progressively less effective [ZHA 95]. However, for the applications where carrier conductivity is required, we should come to the conclusion that the quasi-1D is the optimal dimensionality, and in fact it rivals many living or naturally occurring systems where energy transfer to acceptors occurs through a conduit in the form of a "fiber" or "tube." A solar cell using an array of nanowires (NWs) as its active element for light absorption and carrier transport will be a nanoextension and optimization of the conventional planar device with contact grid lines or the back-contact cell. The major advantage of the NW solar cell lies in that the electron–hole separation can occur in a very short spatial distance; thus, the non-radiative recombination can be more effectively suppressed than in the planar architecture or its variations. Consequently, the quasi-1D device architecture may relax the stringent requirement to material quality. In the meantime, the laterally separated carriers of the opposite types can transport in separated channels along relatively non-restricted vertical paths (the core and shell) to the respective electrodes. There are two primary ways to achieve the lateral charge separation in an NW solar cell: a core–shell p–n junction[KAY 05] and a type II(a) core–shell structure [ZHA 07]. Both types of junctions are expected to function in the mesoscopic scale (i.e. with relatively large NWs), but only the latter can remain functional in the quantum region. Additionally, an NW array may also provide the functionality of light trapping, and thus is capable of simultaneously serving three key functions in the energy production: light trapping, energy conversion and transport. With modifications, the quasi-1D systems could be useful for other solar energy applications, such as hydrogen generation via photo-electrochemical water splitting [ZHA 07]. Figure 4.2 shows schematically the device structure for a solar cell based on an array of type II(a) core–shell NW arrays, as well as the possible electronic transitions that are expected to occur in such a heterostructure. The key aspect for this type of device to function differently from the simple superposition of the two materials lies in having sufficiently strong interfacial optical transition, denoted as E_{g3} in Figure 4.2(b). This transition, practically impossible for a p–n junction due to the large junction width w, has been found to be extremely weak in the organic PV cell [CLA 10] and moderately strong for the type II(b) super-lattice with more than 100 periods [MOU 09]. A similar core–shell NW array structure can in fact be envisioned for the type II(b)

heterostructure with IR detection application in mind. Since our focus is on the type II(a) heterostructure with large bandgap materials for PV-related applications, from now on we simply refer to type II(a) as type II.

4.4. Electronic structure of type II core–shell nanowires

On a qualitative level, we could estimate the type II transition energy using the information of the bulk band alignment and taking into account the possible stress effect. The band diagrams for three systems: GaN–GaP, ZnO–ZnSe and ZnO–ZnTe are shown in Figure 4.3 [ZHA 07, WAN 08]. Qualitatively speaking, we expect that the type II bandgap of ZnO–ZnSe combination should be higher than that of GaN–GaP.

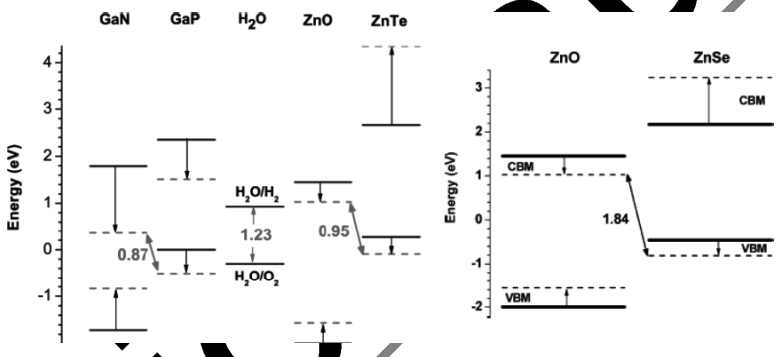

Figure 4.3. *Energy diagrams of bulk GaN, GaP, ZnO, ZnSe, ZnT, and the chemical reaction potential energies of H_2O. Solid lines indicate the band-edge energies (the CBM and VBM) with natural lattice constants, dashed lines with average lattice constants between GaN and GaP, ZnO and ZnSe, and ZnO and ZnTe. Adapted from [ZHA 07,WAN 08]. For a color version of this figure, see www.iste.co.uk/consonni/nanowires2.zip*

The electronic structures of type II core–shell NWs were investigated using a density-functional theory for GaN–GaP and ZnO–ZnSe with the bandgap error due to a corrected local density approximation [ZHA 07]. As anticipated based on the qualitative understanding of the type II band alignment, a core–shell NW indeed yields a new bandgap that is much smaller than any of the components, and shows the key feature of the type II alignment – the CBM and VBM are located respectively in the core and the shell. For instance, for an NW with GaN core and GaP shell and a core diameter of ~1.5 nm and total size ~2.4 nm, both in zinc blende (ZB) structure, the bandgap was found to be only 1.22 eV. Interestingly, the reversed structure with GaP core and GaN shell yielded nearly the same

bandgap, 1.21 eV. Figure 4.4 shows the charge distribution of the CBM and VBM for these core–shell NWs. The results indicate that once the photo-generated electrons and holes relax to the respective band edges, they will be spatially separated into the GaN and GaP regions, respectively. Note that the NWs do not have cylindrical symmetry but are faceted with C_{3V} symmetry, which is manifested in the wave-function plots of Figure 4.4, most apparent for the NW of GaP (core)–GaN (shell). It could be of significant interest to study the angular modulation of the wavefunction for properties relevant to optical and spin polarization.

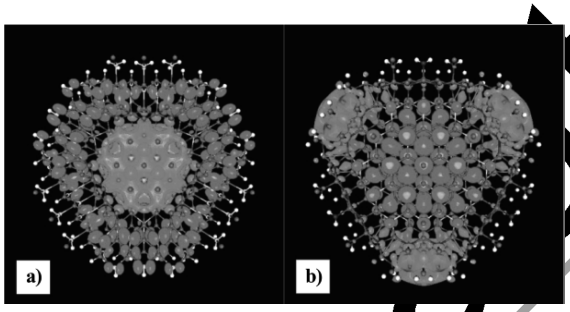

Figure 4.4. *Cross-section views of charge distributions of the CBM electron state (cyan) and VBM hole state (green) superimposed on the atomic structures in zincblende [111] core–shell NWs: a) GaN(core)–GaP(shell); and b) GaP(core)–GaN(shell). The color codes for the atoms are N, blue; P, yellow; Ga, magenta; pseudo-H, white. The horizontal axis is in the zincblende [-1,1,0] direction, and the vertical is [-1,-1,2]. Adapted from [ZHA 07]. For a color version of this figure, see www.iste.co.uk/consonni/nanowires2.zip*

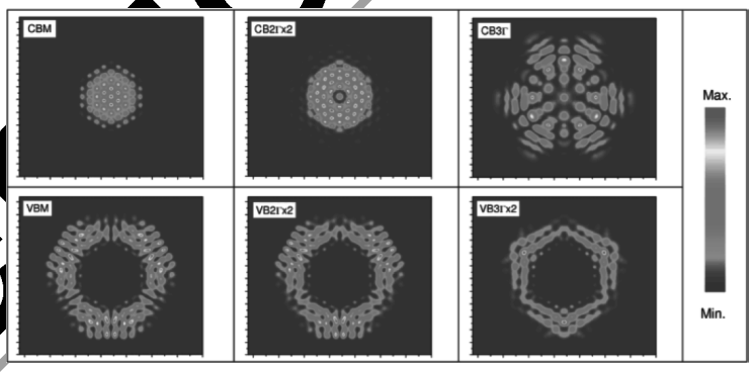

Figure 4.5. *Cross-section views of integrated charge distributions over the wire period for a GaN–GaP core–shell NW. The scale of each frame is 7.70 nm (width) x 6.67 nm (height). Adapted from [ZHA 07]. For a color version of this figure, see www.iste.co.uk/consonni/nanowires2.zip*

The spatial separation of the wave functions implies a small probability for the electron and hole to recombine either radiatively or non-radiatively, thus expecting to yield a long carrier lifetime. A legitimate concern would be that such a structure has weak absorption. However, the electron–hole wave-function overlap increases substantially starting from the secondary bandgap between the second valence sub-band and the first conduction sub-band at around 40–50 meV higher than the fundamental bandgap for the two core–shell structures mentioned above. Figure 4.2 depicts the Γ point wavefunctions for the first few conduction and valence sub-bands for the GaN–GaP NW, showing the electron wavefunctions gradually expand into the shell, whereas the hole wavefunctions gradually invade the core. These types of systems could be potentially of great interest for exploring high mobility quasi-1D electron and hole gases.

The electronic structure of the core–shell NW can be tuned by changing either the core–shell ratio or the overall size. For the GaP–GaN core–shell NW mentioned above with $E_g \approx 1.21$ eV, if keeping the same GaP core size but increasing the shell thickness to the total diameter ~3.1 nm, the bandgap will increase to 1.45 eV.

ZnO–ZnSe-based core–shell NWs tend to have somewhat larger bandgaps than those of GaN–GaP core–shell NWs of comparable sizes, as already suggested by the simple estimates shown in Figure 4.3. For instance, with the same numbers of atomic layers in the core and shell, the bandgap of the GaN–GaP NW was calculated to be about 1.22 eV as mentioned above; it became close to 2 eV for the ZnO–ZnSeNWs. The bandgaps of the core–shell NW of ZnO–ZnS are expected to be even larger [SCH 07].

In reality, it remains challenging to grow core–shell NWs of the sizes that are convenient for theoretical modeling and at which the quantum confinement effects are significant. However, the basic function of the type II interface – separating the electrons and holes – continues to exist for larger sizes, except for losing the possibility of bandgap structure engineering. Also, for the large size, the absorption near the type II bandgap relies truly on the interfacial effect which is expected to be rather weak for a long core–shell NW. However, in the form of a dense array of a proper density and height, light trapping effect can significantly increase the optical path due to inter-wire scattering. Together with the enhanced surface area, which is proportion to the ratio of the length to diameter, the device can in principle have enough absorption, likely better than the situation in a thin-film Si solar cell with surface texturing.

Clearly even without doping, the core–shell NW can already function as a lateral p–n junction. However, doping can provide further tunability in material properties. The large bandgap materials like GaN and ZnO tend to be naturally n-type, which will not affect the basic functionality of the type II hetero-junction, unless they would become p-type. We can have the flexibility to place either component as core or shell, depending on the targeted application. For instance, in the case of hydrogen generation via photo-electrochemical water splitting, using GaN shell is expected to provide better chemical stability than the reversed structure [BEA 03].

4.5. Synthesis of the type II core–shell nanowires and their signatures

The synthesis of GaN–GaP and GaP–GaN core–shell NWs was perhaps the first effort reported for the fabrication of type II core–shell NWs [LI 03], although it might not be in the context of seeking any property associated with the type II band alignment. Following the initial proposal of exploring the type II core–shell NW for solar energy-related applications [ZHA 07], vertically aligned ZnO(core)–ZnSe(shell) NW arrays were successfully grown on indium tin oxide (ITO) substrates using CVD for the ZnO core and PLD for the ZnSe shell [WAN 08]. The details for this catalyst-free growth can be found in the original paper [WAN 08]. The readers may also consult Chapter 11 in Vol. 1 [CON 14] for more general discussions. The characterization results are summarized in Figure 4.6. Figure 4.6(a) and (b) shows, respectively, the SEM images of the ZnO NW array before and after coated with ZnSe. The single crystalline ZnO NW core, approximately 100 nm in size and 10 μm in length, was found to be in the wurtzite (WZ) c-axis. However, the polycrystalline ZnSe shell, approximately 5–8 nm in thickness, was in ZB phase with epitaxial relationship $[0001]_{ZnO}//[0\bar{1}1]_{ZnSe}$ and $[2\text{-}1\text{-}10]_{ZnO}//(011)_{ZnSe}$, as revealed in Figure 4.6(d). Although bulk ZnSe is typically observed in ZB phase, ZnSe in WZ phase is also possible. If both were in WZ phase, the lattice mismatch would be approximately 25% with respect to that of ZnO, which is even larger than the mismatch between GaN and GaP (below 20%). However, the lattice constant of the ZB ZnSe is only 8.8% larger than the c-axis lattice constant of the WZ ZnO. Despite the ZnSe shell being rather thin, the ZnO core was found to be stretched by the shell, as shown by the x-ray diffraction (XRD) data in Figure 4.6(c). The core–shell NW did show the optical signatures of the individual components, such as the respective excitonic absorption peaks, Figure 4.6(e), and Raman modes for both ZnO and ZnSe, Figure 4.6(f), but no clear evidence of the expected signatures of a type II heterostructure. Nevertheless, the results were encouraging and significant, because it demonstrated the feasibility of growing a highly mismatched heterostructure in the quasi-1D geometry otherwise not possible in the 2D planar geometry.

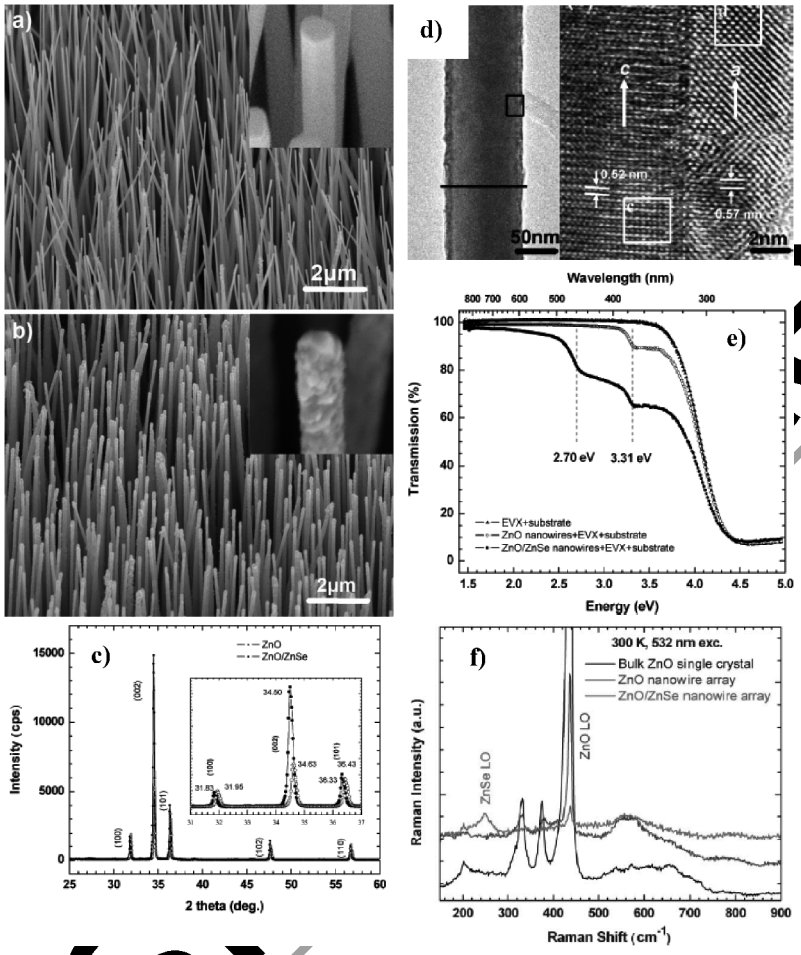

Figure 4. *Vertically aligned ZnO–ZnSe core–shell NW array grown on TCO substrate. a) SEM image of the ZnO NWs; b) SEM image of the ZnO–ZnSe core–shell NWs. The insets in a) and b) are enlarged images of ZnO NW tips and a core – shell NW tip, respectively; c) XRD patterns of ZnO and ZnO–ZnSe NW arrays. The inset shows a clear shift of the peaks to the smaller angle side on going from ZnO to ZnO–ZnSe; d) low-magnification TEM image of a ZnO–ZnSe core/shell NW (left), showing a thin layer of ZnSe coated on the ZnO NW core, and high-resolution TEM image of the interface of the core–shell heterostructure (right), enlarged from the rectangular area outlined in the image on the left, showing the epitaxial growth relationship of the ZnO WZ core and ZnSe ZB shell; e) transmission spectra of ZnO NWs and the corresponding ZnO–ZnSe core–shell NWs. The two vertical lines indicate the excitonic bandgaps of bulk ZnO and ZnSe. NWs were dispersed in the dilute solution of EVX (ethylene–vinyl acetate copolymer); f) Raman spectra of ZnO and ZnO–ZnSeNW arrays, compared with that of a bulk ZnO single crystal. Adapted from [WAN 08]. For a color version of this figure, see www.iste.co.uk/consonni/nanowires2.zip*

What would be considered as the signatures or evidence of a type II heterostructure? The common accepted signatures might include: (1) a photoluminescence (PL) peak at the expected interfacial transition energy that should be below the lower bandgap of the two components; (2) optical absorption occurring in the spectral region of the anticipated interfacial transition, which is expected to extend into the longer wavelength than the threshold determined by the bandgap of the lower bandgap component; (3) a long carrier time or slow decay of the type II emission; and (4) photo-response (i.e. photo-current) associated with the type II transition. The signature (1) alone might not be reliable, because defects in either component could potentially also result in below bandgap emission. Signature (2) is more reliable than (1), because the defects are less unlikely to have any measureable absorption strength, unless with a very high density? Signature (3) is usually viewed as more reliable, because a defect state in the bulk part of the material rarely has a long lifetime. In fact, the presence of defects in the bulk part tends to shorten the carrier lifetime. The observation of a long carrier lifetime could be viewed as an indication of good quality of the material involved. It is worth pointing out that if a defect is formed at the type II interface, because the electron and hole wavefunctions do not overlap substantially there, the carriers will not easily be captured by the defect, and therefore the defect will not be as detrimental to the carriers as the bulk defects. In this case, we might as well view the interface defect-related transition as a type II transition. Signature (4) would be an ultimate confirmation of the type II effect, although there is the possibility that the photo-response could be due to the interfacial defect. There is also a remote possibility that the photo-excitation of a defect or an impurity state in the bulk part of the heterostructure could tunnel out through the type II interface.

4.6. Demonstration of type II effects in ZnO–ZnSe core–shell nanowires and photovoltaic devices

Another attempt of growing ZnO–ZnSe core–shell NWs has led to the observation of all the four signatures mentioned above of a type II hetero-junction [WU 11, ZHA 11]. In addition, it reports a very different epitaxial growth of ZnSe shell on ZnO core from the first attempt [WAN 08]. Instead of growing on ITO substrate [WAN 08], the ZnO NWs were grown by CVD on a ZnO buffer layer that was deposited on a quartz glass by MBE. The ZnO NWs are 40–80 nm in size and about 1.5 μm long. Polycrystalline ZnSe shell was coated by CVD with approximate thickness of 50 nm, which is substantially thicker than that in the other report. The typical morphologies of the as-grown ZnO NW array and ZnO/ZnSe core–shell NW array are shown in Figure 4.7 [WU 11].

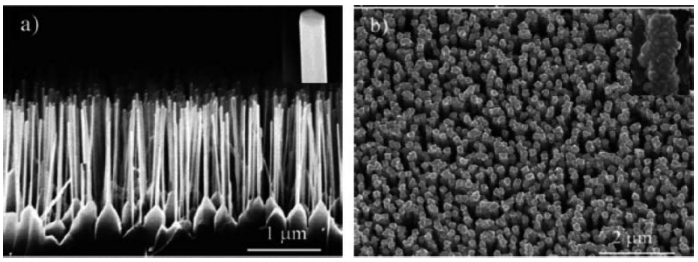

Figure 4.7. *SEM images of a) as grown ZnO NWs and b) ZnO–ZnSe core–shell NWs. The insets in a) and b) are high-magnification SEM images of a single ZnO and ZnO–ZnSe core–shell NW, respectively. Adapted from [WU 11]*

In contrast to the epitaxial relationship of $[0001]_{ZnO}//[0001]_{ZnSe}$ observed in the first synthesis, this time the ZnSe shell was found to be also in the WZ phase and have the same lattice constant of ZnO, with an epitaxial relationship of $[0001]_{ZnO}//[0001]_{ZnSe}$, when the shell thickness is in the range 2–12 nm. Beyond that, the ZnSe shell relaxed into the ZB phase with its [111] axis parallel to the WZ [0001] axis. Figure 4.8 shows the TEM images of a typical ZnO–ZnSe core–shell NW [WU 11]. It is an astonishing finding that with ~25% compressive strain, the ZnSe shell was actually grown coherently on the ZnO core. The size difference of the ZnO NW core between the two attempts could be the primary reason for the observed different epitaxial relationships, because the smaller ZnO core of the second attempt likely made the highly strained epitaxial deposition of ZnSe of the same phase and orientation somewhat easier. The smaller ZnO core is perhaps also the key factor for the enhanced type II optical transition to be described below, because on the one hand the interfacial area is enhanced due to the higher NW density; on the other hand the electronic coupling at the interface could also be improved. Both the growth mechanism and electronic properties of these non-conventional heterostructures are not well understood at this time and deserve careful investigation in the future.

The first two signatures of the type II hetero-junction, below bandgap emission and absorption, were observed for the core–shell structure, as shown in Figure 4.9 [WU 11]. The emission peak at around 1.9 eV is a reasonable energy for the type II transition of this system (see Figure 4.3), and the weakening of the ZnO band edge peak could be explained as due to the charge transfer effect, although the PL measurement alone is not reliable for drawing the conclusion. The transmission spectra further supports the suggestion that the core–shell structure does give rise to type II optical transition, as it is clear that the absorption of the core–shell NW array now extends well into the longer wavelength range even reaching near IR.

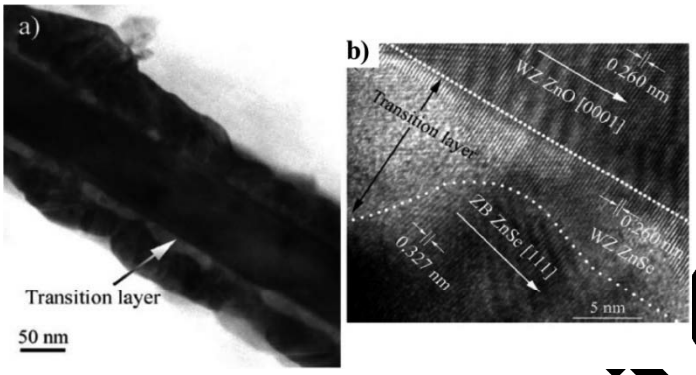

Figure 4.8. *TEM images of a ZnO–ZnSe core–shell NW. a) Low-magnification image with the transition layer being WZ ZnSe; b)high-resolution image of the interface between the ZnO core and the ZnSe shell. Adapted from [WU 11].*

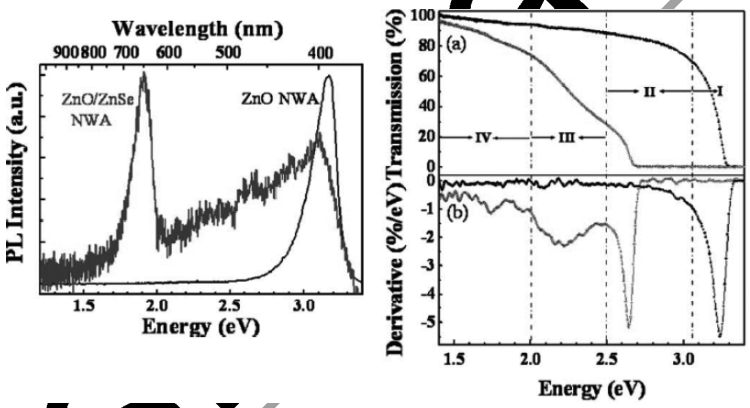

Figure 4.9. *Type II optical transitions of ZnO–ZnSe core–shell NWs. Left –normalized PL spectra for ZnO and ZnO–ZnSe core–shell NW arrays. Right – a) transmission spectra of ZnO NWs (black) and ZnO–ZnSe core–shell NWs (blue); and b) derivative curves of the transmission spectra a). I – the inter-band transition of ZnO, II – the inter-band transition of ZnSe, III – interfacial transition between ZnO and ZB–ZnSe and IV – the interfacial transition between ZnO and WZ–ZnSe. Adapted from [WU 11]. For a color version of this figure, see www.iste.co.uk/consonni/nanowires2.zip*

The third signature – the long carrier lifetime of the interfacial transition – has also been observed for the core–shell NW array, which adds more certainty on the existence of the type II optical transition in this system [ZHA 12]. Figure 4.10 shows the time resolved PL at different energies across a broad emission band for a ZnO–

ZnSe core–shell NW sample at low temperature, together with a time-averaged PL spectrum, all measured at ~8K. Although not measured from the same sample used in Figure 4.9, the peak energy of the type II transition is found to be around 2.03 eV at 8 K, which is consistent with the room temperature value of ~1.9 eV, if we take into account the temperature dependence of the bandgap energy (typically ~100 meV between 0 and 300 K). The time-dependent data show periodic modulations with very little decay within each time window of 13.16 ns determined by the repetition rate of the laser. The time-dependent data clearly indicate long PL decay times for various optical transitions in the whole broad spectral range. Fitting the curve of 2.045 eV (near the peak of the broad band) using a function form with a single exponential decay term but taking into account repeating excitations, an estimated decay time of ~64 ns was obtained. This decay time is more than two orders of magnitude longer than the typical radiative decay time in a direct bandgap semiconductor at low temperature (typically a few hundred ps). A weak peak at ~2.70 eV, which is below the bandgap energy of 2.80 eV for ZnSe [WAL 96], also shows a relatively slow decay, with a decay time ~20 ns. This transition was suggested to be related to the interfacial transition of ZnO–ZnSe–GaN–ZnSe that is expected to also have a type II band alignment [WU 11].

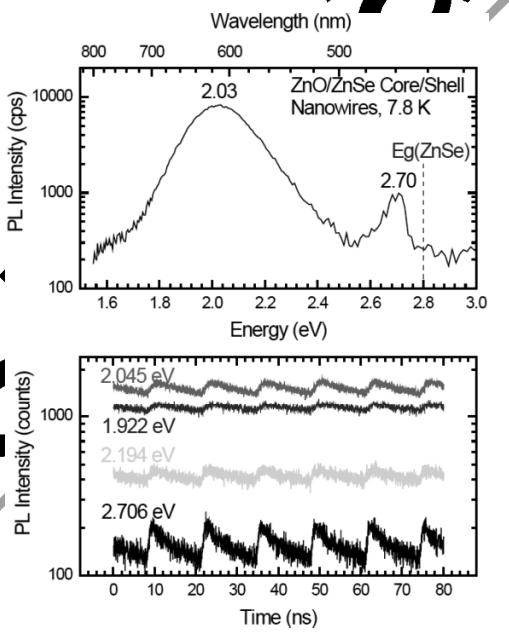

Figure 4.10. *Time-resolved photoluminescence measured at low temperature. (Top) Time-averaged spectrum, (bottom) decay curves monitored at different emission energies. Adapted from [ZHA 12]. For a color version of this figure, see www.iste.co.uk/consonni/nanowires2.zip*

The ultimate confirmation for the type II functionality of the ZnO–ZnSe core–shell NW hetero-junction was provided by a proof-of-concept PV device that was realized by adding an electrode to the ZnO buffer layer and pressing an ITO electrode on top of the NW array. Figure 4.11 shows the basic optoelectronic characterization results for the prototype PV cell [WU 11]: EQE versus light wavelength, and open-circuit voltage (V_{oc}) versus illumination density. As expected, the device clearly shows photo-response in the energy range well below the bandgap of ZnSe, with a peak energy at ~1.9 eV and a threshold at ~1.6 eV. The EQE in the red spectrum reaches about 4%, which is comparable to the maximum of about 9% in the violet spectral range. The relatively low absolute EQE value was likely due to the fact that both electrical contacts were not of high quality. However, the comparable efficiencies between the NIR and the UV spectral ranges suggest that such a device could potentially achieve much higher efficiency, because the EQE in the ZnO spectral range should in principle be much higher than the result achieved on this prototype device, likely due to the primitive forms of contacts. For the illumination density dependence of V_{oc}, the initial rapid increase reflects the adversary effect of defects. Ideally, it should saturate quickly by approaching the dependence of $\ln(I_{sc}/I_0)$, with I_{sc} and I_0 being short-circuit current and dark current, respectively, as shown by the curve for a reference Si cell. The curve for the NW device does not saturate as fast, but V_{oc} reaches a rather high value of 0.70 V at 660 μW/cm^2 (a fairly low power density compared to that of AM 1.5 solar spectrum, ~100 mW/cm^2). This open-circuit voltage is probably one of the highest values achieved thus far for nanostructured PV devices. These results point to the great potential for this novel device concept and architecture.

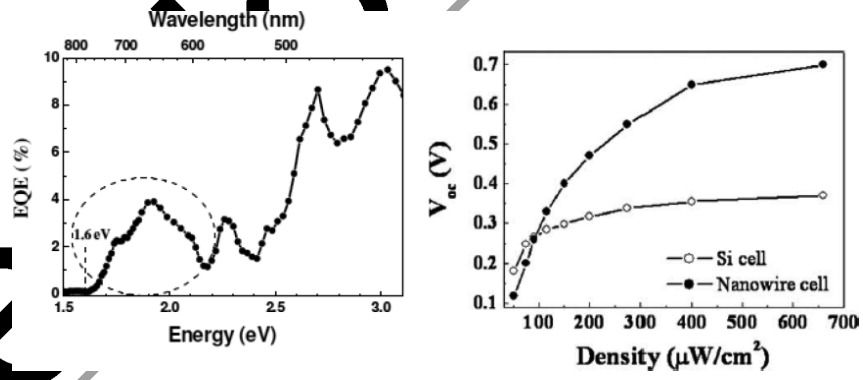

Figure 4.11. *Characterizations of a ZnO–ZnSe core–shell NW array solar cell. Left external quantum efficiency (EQE) versus photon energy; right – open-circuit voltage (V_{oc}) versus illumination density. Adapted from [WU 11]*

To improve the device performance, the improvement is much needed in making better electrical contacts, for instance, by using the planarization technique that has been adopted for the ETA cell (e.g. filling the NW gaps with p-CuSCN) [LEV 05]. Furthermore, the structural parameters of the NW array (e.g. density and height) should be optimized to improve light trapping in order to mitigate relatively weak interfacial absorption.

In addition to the GaN–GaP and ZnO–ZnSe core–shell NWs mentioned above, a number of other type II core–shell NWs with different core–shell combinations have also been synthesized, and the corresponding PV devices have been fabricated in the context of the ETA cell, for instance, ZnO–CdSe [LEV 05] and ZnO–CdTe [WAN 10]. However, so far the ZnO–ZnSe combination is the only one that has been demonstrated with photo-response associated with the type II effect in the form of a core–shell NW [WU 11].

4.7. Summary

A brief review has been provided to highlight an all-inorganic version type II hetero-junction solar cell idea based on large bandgap semiconductors, in particular ZnO–ZnSe and GaN–GaP. In contrast to other well-known type II hetero-junction solar cells, such as BHJSC and DSSC (and their variations) where usually only the lower bandgap material plays the primary role of light absorber, this new type II hetero-junction solar cell emphasizes the utilization of the collaborative effect of the two components, which creates an effective bandgap that can be much smaller than those of the individual components. In these systems, we cannot only take advantage of the better photo- and chemical stability of the large bandgap material, often serving as passivation or window layers, but can also use them as the light absorber. It is as though they mutually sensitize each other. The core–shell NW device architecture has been proposed as the optimal device structure for PV and photo-detection-related optoelectronic devices. The combination of ZnO–ZnSe has been selected to demonstrate the expected signature properties of a type II hetero-junction, including type II emission and absorption, long carrier lifetime, and ultimately type II photo-response. The preliminary device testing results indicate great potential for further improvement and development of the type II core–shell NW-based optoelectronic devices. With the successful demonstrations of the material growth, especially of the highly lattice mismatched epitaxial structures, the basic physical properties of the type II hetero-junction and the device realization, fundamental science investigation is expected to follow, which is currently lacking behind, for instance, the growth mechanism, interfacial states and defects, effects of doping, transport properties and 3D device operation.

4.8. Acknowledgments

The author would like to thank the support of Bissell Distinguished Professorship at UNC-Charlotte, and of "Chairs of Excellence" of "Fondation Nanosciences" (France) during his summer visit (2009–2012) at CEA-CNRS-UJF/NPSC group in Grenoble. He is very grateful to many collaborators who have contributed to the work summarized in this chapter, in particular to those co-authors in the joint publications listed as references [ZHA 07, WAN 08, WU 11, ZHA 12] at NREL (Drs. John Pern, Yanfa Yan and Angelo Mascarenhas), LBNL (Dr. L. Wang Wang), UNO (Drs. Kai Wang and Jiajun Chen, Professor Wei Zhou), Xiamen University (Professors Zhiming Wu and Junyong Kang) and of the NPSC group (Drs. Joel Bleuse and Henri Mariette).

4.9. Bibliography

[BEA 03] BEACH J.D., COLLINS R.T., TURNER J.A., "Band edge positions of n-Type and p-Type GaN", *Journal of The Electrochemical Society*, vol. [illegible], p. A899, 2003.

[BOY 12] BOYER-RICHARD S., ROBERT C., GERARD L., *et al.*, "Atomistic simulations of the optical absorption of type-II CdSe/ZnTe superlattices", *Nanoscale Research Letters*, vol. 7, p. 543, 2012.

[CLA 10] CLARKE T.M., DURRANT J.R., "Charge photogeneration in organic solar cells", *Chemical Reviews*, vol. 110, p. 67[illegible] 2010.

[CON 14] CONSONNI V., FEUILLET G. (eds), *Wide Band Gap Semiconductor Nanowires 1: Low-Dimensionality Effects and Growth*, ISTE, London, John Wiley & Sons, New York, 2014.

[ERN 03] ERNST K., BELAIDI A., KÖNENKAMP R., "Solar cell with extremely thin absorber on highly structured substrate", *Semiconductor Science and Technology*, vol. 18, p. 475, 2003.

[GRA 01] GRÄTZEL M., "Photoelectrochemical cells", *Nature*, vol. 414, p. 338, 2001.

[KAY 05] KAYES B.M., ATWATER H.A., LEWIS N.S., "Comparison of the device physics principles of planar and radial p-n junction nanorod solar cells", *Journal of Applied Physics*, vol. 97, p. 114302, 2005.

[KRO 01] KROEMER H., "Quasi-electric fields and band offsets: teaching electrons", in EKSTEN G. (ed.), *Nobel Lectures*, World Scientific Publishing, p. 449, 2002.

[LEV 05] LEVY-CLEMENT C., TENA-ZAERA R., RYAN M.A., *et al.*, "CdSe-sensitized p-CuSCN/nanowire n-ZnO heterojunctions", *Advanced Materials*, vol. 17, p. 1512, 2005.

[LI 09] LI Y.-H., WALSH A., CHEN S., *et al.*, "Revised ab initio natural band offsets of all group IV, II-VI, and III-V semiconductors", *Applied Physics Letters*, vol. 94, 2009.

[LIN 03] LIN H.M., CHEN Y.L., YANG J., *et al.*, "Synthesis and characterization of core-shell GaP @ GaN and GaN@GaP nanowires", *Nano Letters*, vol. 3, p. 537, 2003.

[MAL 96] MALIKOVA L., KRYSTEK W., POLLAK F.H., *et al.*, "Temperature dependence of the direct gaps of ZnSe and Zn{0.56}Cd{0.44}Se", *Physical Review B*, vol. 54, p. 1819, 1996.

[MIL 97] MILLUNCHICK J.M., TWESTEN R.D., LEE S.R., *et al.*, "Spontaneous lateral composition modulation in AlAs/InAs short period superlattices via the growth front", *Journal of Elec Materi*, vol. 26, p. 1048, 1997.

[MOU 09] MOU S., LI J.V., CHUANG S.L., "Quantum efficiency analysis of InAs–GaSb Type-II superlattice photodiodes", *IEEE Journal of Quantum Electronics*, vol. 45, p. 1, 2009.

[NEL 02] NELSON J., "Organic photovoltaic films", *Current Opinion in Solid State and Materials Science*, vol. 6, p. 87, 2002.

[SCH 07] SCHRIER J., DEMCHENKO D.O., WANG L.W., "Optical properties of ZnO/ZnS and ZnO/ZnTe heterostructures for photovoltaic applications", *Nano Letters*, vol. 7, p. 2377, 2007.

[SWA 86] SWANSON R.M., "Point-contact solar cells: modeling and experiment", *Solar Cells*, vol. 17, p. 85, 1986.

[VAN 03] VAN DE WALLE C.G., NEUGEBAUER J., "Universal alignment of hydrogen levels in semiconductors, insulators and solutions", *Nature*, vol. 423, p. 626, 2003.

[WAN 08] WANG K., CHEN J., ZHOU W., *et al.*, "Direct growth of ZnO/ZnSe highly mismatched type II core/shell nanowire arrays on transparent conducting oxide (TCO) substrate for potential solar cell application", *Advanced Materials*, vol. 20, p. 3248, 2008.

[WAN 10] WANG X., ZHU J., XU Y., *et al.*, "Designed ZnO/CdTe core–shell nanocable arrays on indium tin oxide: synthesis and photoelectrochemical properties", *ACS Nano*, vol. 4, p. 3302, 2010.

[WU 11] WU Z., ZHANG Y., ZHENG J., *et al.*, "An all-inorganic Type-II heterojunction array with near-full solar spectral response based on ZnO/ZnSe core/shell nanowires", *Journal of Materials Chemistry*, vol. 21, p. 6020, 2011.

[YU 06] YU P.R., ZHU K., NORMAN A.G., *et al.*, "Nanocrystalline TiO2 solar cells sensitized with InAs quantum dots", *Journal of Physical Chemistry B*, vol. 110, p. 25451, 2006.

[ZHA 95] ZHANG Y., STURGE M.D., KASH K., *et al.*, "Temperature dependence of luminescence efficiency, exciton transfer, and exciton localization in GaAs/Al{x}Ga{1-x}As quantum wires and quantum dots", *Physical Review B*, vol. 51, p. 13303, 1995.

[ZHA 07] ZHANG Y., WANG L.-W., MASCARENHAS A., "Quantum coaxial cables for solar energy harvesting", *Nano Letters*, vol. 7, p. 1264, 2007.

[ZHA 12] ZHANG Y., WU Z., ZHENG J., *et al.*, "ZnO/ZnSe type II core–shell nanowire array solar cell", *Solar Energy Materials and Solar Cells*, vol. 102, vol. 15, 2012.